

Energy scan of the $e^+e^- \rightarrow h_b(nP)\pi^+\pi^-$ ($n = 1, 2$) cross sections and evidence for $\Upsilon(11020)$ decays into charged bottomonium-like states

I. Adachi,^{13,9} H. Aihara,⁶⁸ D. M. Asner,⁵² H. Atmacan,³⁸ V. Aulchenko,^{3,50} T. Aushev,⁴¹ R. Ayad,⁶¹ I. Badhrees,^{61,25} A. M. Bakich,⁶⁰ E. Barberio,³⁷ P. Behera,¹⁷ V. Bhardwaj,⁵⁸ B. Bhuyan,¹⁶ J. Biswal,²² A. Bobrov,^{3,50} A. Bondar,^{3,50} G. Bonvicini,⁷³ A. Bozek,⁴⁷ M. Bračko,^{35,22} T. E. Browder,¹² D. Červenkov,⁴ V. Chekelian,³⁶ A. Chen,⁴⁴ B. G. Cheon,¹¹ K. Chilikin,^{31,40} R. Chistov,^{31,40} V. Chobanova,³⁶ S.-K. Choi,¹⁰ Y. Choi,⁵⁹ D. Cinabro,⁷³ J. Dalseno,^{36,63} M. Danilov,^{40,31} N. Dash,¹⁵ Z. Doležal,⁴ A. Drutskoy,^{31,40} S. Eidelman,^{3,50} D. Epifanov,⁶⁸ T. Ferber,⁶ B. G. Fulsom,⁵² V. Gaur,⁶² A. Garmash,^{3,50} R. Gillard,⁷³ Y. M. Goh,¹¹ P. Goldenzweig,²⁴ B. Golob,^{32,22} D. Greenwald,⁶⁴ T. Hara,^{13,9} K. Hayasaka,⁷⁶ H. Hayashii,⁴³ W.-S. Hou,⁴⁶ C.-L. Hsu,³⁷ K. Inami,⁴² G. Inguglia,⁶ A. Ishikawa,⁶⁶ Y. Iwasaki,¹³ I. Jaegle,¹² T. Julius,³⁷ K. H. Kang,²⁹ P. Katrenko,^{41,31} D. Y. Kim,⁵⁷ H. J. Kim,²⁹ J. B. Kim,²⁷ K. T. Kim,²⁷ M. J. Kim,²⁹ S. H. Kim,¹¹ Y. J. Kim,²⁶ K. Kinoshita,⁵ P. Kodyš,⁴ S. Korpar,^{35,22} D. Kotchetkov,¹² P. Krokovny,^{3,50} T. Kuhr,³³ A. Kuzmin,^{3,50} Y.-J. Kwon,⁷⁵ J. S. Lange,⁸ C. H. Li,³⁷ H. Li,¹⁸ L. Li,⁵⁴ L. Li Gioi,³⁶ J. Libby,¹⁷ D. Liventsev,^{72,13} M. Lubej,²² T. Luo,⁵³ M. Masuda,⁶⁷ T. Matsuda,³⁹ D. Matvienko,^{3,50} K. Miyabayashi,⁴³ H. Miyata,⁴⁹ R. Mizuk,^{31,40,41} G. B. Mohanty,⁶² A. Moll,^{36,63} E. Nakano,⁵¹ M. Nakao,^{13,9} T. Nanut,²² K. J. Nath,¹⁶ K. Negishi,⁶⁶ M. Niyama,²⁸ N. K. Nisar,^{62,1} S. Nishida,^{13,9} S. Ogawa,⁶⁵ S. Okuno,²³ S. L. Olsen,⁵⁵ Y. Onuki,⁶⁸ P. Pakhlov,^{31,40} G. Pakhlova,^{31,41} B. Pal,⁵ C. W. Park,⁵⁹ H. Park,²⁹ S. Paul,⁶⁴ T. K. Pedlar,³⁴ R. Pestotnik,²² M. Petrič,²² L. E. Pilonen,⁷² C. Pulvermacher,²⁴ M. Ritter,³³ Y. Sakai,^{13,9} S. Sandilya,⁵ T. Sanuki,⁶⁶ V. Savinov,⁵³ T. Schlüter,³³ O. Schneider,³⁰ G. Schnell,^{2,14} C. Schwanda,²⁰ Y. Seino,⁴⁹ D. Semmler,⁸ K. Senyo,⁷⁴ O. Seon,⁴² M. E. Sevier,³⁷ V. Shebalin,^{3,50} T.-A. Shibata,⁶⁹ J.-G. Shiu,⁴⁶ B. Shwartz,^{3,50} F. Simon,^{36,63} E. Solovieva,^{31,41} M. Starič,²² J. Stypula,⁴⁷ T. Sumiyoshi,⁷⁰ M. Takizawa,⁵⁶ U. Tamponi,^{21,71} K. Tanida,⁵⁵ Y. Teramoto,⁵¹ I. Tikhomirov,⁴⁰ K. Trabelsi,^{13,9} M. Uchida,⁶⁹ T. Uglov,^{31,41} Y. Unno,¹¹ S. Uno,^{13,9} P. Urquijo,³⁷ Y. Usov,^{3,50} C. Van Hulse,² G. Varner,¹² V. Vorobyev,^{3,50} C. H. Wang,⁴⁵ M.-Z. Wang,⁴⁶ P. Wang,¹⁹ X. L. Wang,⁷² Y. Watanabe,²³ K. M. Williams,⁷² E. Won,²⁷ J. Yamaoka,⁵² Y. Yamashita,⁴⁸ J. Yelton,⁷ C. Z. Yuan,¹⁹ Z. P. Zhang,⁵⁴ V. Zhilich,^{3,50} V. Zhukova,⁴⁰ V. Zhulanov,^{3,50} and A. Zupanc^{32,22}

(The Belle Collaboration)

¹Aligarh Muslim University, Aligarh 202002

²University of the Basque Country UPV/EHU, 48080 Bilbao

³Budker Institute of Nuclear Physics SB RAS, Novosibirsk 630090

⁴Faculty of Mathematics and Physics, Charles University, 121 16 Prague

⁵University of Cincinnati, Cincinnati, Ohio 45221

⁶Deutsches Elektronen-Synchrotron, 22607 Hamburg

⁷University of Florida, Gainesville, Florida 32611

⁸Justus-Liebig-Universität Gießen, 35392 Gießen

⁹SOKENDAI (The Graduate University for Advanced Studies), Hayama 240-0193

¹⁰Gyeongsang National University, Chinju 660-701

¹¹Hanyang University, Seoul 133-791

¹²University of Hawaii, Honolulu, Hawaii 96822

¹³High Energy Accelerator Research Organization (KEK), Tsukuba 305-0801

¹⁴IKERBASQUE, Basque Foundation for Science, 48013 Bilbao

¹⁵Indian Institute of Technology Bhubaneswar, Satya Nagar 751007

¹⁶Indian Institute of Technology Guwahati, Assam 781039

¹⁷Indian Institute of Technology Madras, Chennai 600036

¹⁸Indiana University, Bloomington, Indiana 47408

¹⁹Institute of High Energy Physics, Chinese Academy of Sciences, Beijing 100049

²⁰Institute of High Energy Physics, Vienna 1050

²¹INFN - Sezione di Torino, 10125 Torino

²²J. Stefan Institute, 1000 Ljubljana

²³Kanagawa University, Yokohama 221-8686

²⁴Institut für Experimentelle Kernphysik, Karlsruhe Institut für Technologie, 76131 Karlsruhe

²⁵King Abdulaziz City for Science and Technology, Riyadh 11442

²⁶Korea Institute of Science and Technology Information, Daejeon 305-806

²⁷Korea University, Seoul 136-713

²⁸Kyoto University, Kyoto 606-8502

²⁹Kyungpook National University, Daegu 702-701

³⁰École Polytechnique Fédérale de Lausanne (EPFL), Lausanne 1015

- ³¹*P.N. Lebedev Physical Institute of the Russian Academy of Sciences, Moscow 119991*
³²*Faculty of Mathematics and Physics, University of Ljubljana, 1000 Ljubljana*
³³*Ludwig Maximilians University, 80539 Munich*
³⁴*Luther College, Decorah, Iowa 52101*
³⁵*University of Maribor, 2000 Maribor*
³⁶*Max-Planck-Institut für Physik, 80805 München*
³⁷*School of Physics, University of Melbourne, Victoria 3010*
³⁸*Middle East Technical University, 06531 Ankara*
³⁹*University of Miyazaki, Miyazaki 889-2192*
⁴⁰*Moscow Physical Engineering Institute, Moscow 115409*
⁴¹*Moscow Institute of Physics and Technology, Moscow Region 141700*
⁴²*Graduate School of Science, Nagoya University, Nagoya 464-8602*
⁴³*Nara Women's University, Nara 630-8506*
⁴⁴*National Central University, Chung-li 32054*
⁴⁵*National United University, Miao Li 36003*
⁴⁶*Department of Physics, National Taiwan University, Taipei 10617*
⁴⁷*H. Niewodniczanski Institute of Nuclear Physics, Krakow 31-342*
⁴⁸*Nippon Dental University, Niigata 951-8580*
⁴⁹*Niigata University, Niigata 950-2181*
⁵⁰*Novosibirsk State University, Novosibirsk 630090*
⁵¹*Osaka City University, Osaka 558-8585*
⁵²*Pacific Northwest National Laboratory, Richland, Washington 99352*
⁵³*University of Pittsburgh, Pittsburgh, Pennsylvania 15260*
⁵⁴*University of Science and Technology of China, Hefei 230026*
⁵⁵*Seoul National University, Seoul 151-742*
⁵⁶*Showa Pharmaceutical University, Tokyo 194-8543*
⁵⁷*Soongsil University, Seoul 156-743*
⁵⁸*University of South Carolina, Columbia, South Carolina 29208*
⁵⁹*Sungkyunkwan University, Suwon 440-746*
⁶⁰*School of Physics, University of Sydney, New South Wales 2006*
⁶¹*Department of Physics, Faculty of Science, University of Tabuk, Tabuk 71451*
⁶²*Tata Institute of Fundamental Research, Mumbai 400005*
⁶³*Excellence Cluster Universe, Technische Universität München, 85748 Garching*
⁶⁴*Department of Physics, Technische Universität München, 85748 Garching*
⁶⁵*Toho University, Funabashi 274-8510*
⁶⁶*Department of Physics, Tohoku University, Sendai 980-8578*
⁶⁷*Earthquake Research Institute, University of Tokyo, Tokyo 113-0032*
⁶⁸*Department of Physics, University of Tokyo, Tokyo 113-0033*
⁶⁹*Tokyo Institute of Technology, Tokyo 152-8550*
⁷⁰*Tokyo Metropolitan University, Tokyo 192-0397*
⁷¹*University of Torino, 10124 Torino*
⁷²*Virginia Polytechnic Institute and State University, Blacksburg, Virginia 24061*
⁷³*Wayne State University, Detroit, Michigan 48202*
⁷⁴*Yamagata University, Yamagata 990-8560*
⁷⁵*Yonsei University, Seoul 120-749*
⁷⁶*Kobayashi-Maskawa Institute, Nagoya University, Nagoya 464-8602*

(Dated: June 10, 2016)

Using data collected with the Belle detector at the KEKB asymmetric-energy e^+e^- collider, we measure the energy dependence of the $e^+e^- \rightarrow h_b(nP)\pi^+\pi^-$ ($n = 1, 2$) cross sections from thresholds up to 11.02 GeV. We find clear $\Upsilon(10860)$ and $\Upsilon(11020)$ peaks with little or no continuum contribution. We study the resonant substructure of the $\Upsilon(11020) \rightarrow h_b(nP)\pi^+\pi^-$ transitions and find evidence that they proceed entirely via the intermediate isovector states $Z_b(10610)$ and $Z_b(10650)$. The relative fraction of these states is loosely constrained by the current data: the hypothesis that only $Z_b(10610)$ is produced is excluded at the level of 3.3 standard deviations, while the hypothesis that only $Z_b(10650)$ is produced is not excluded at a significant level.

PACS numbers: 14.40.Rt, 14.40.Pq, 13.66.Bc

Heavy quarkonium is a bound state of the $c\bar{c}$ or $b\bar{b}$ quarks. The heavy quarks are moving relatively slowly; therefore, a non-relativistic approximation based on the interaction potential accurately describes the basic prop-

erties of this system [1]. The first state that did not fit potential model expectations was observed in 2003 by Belle [2]; since then, almost twenty such states have been reported [3]. They correspond to high excitations and

have masses above the $D\bar{D}$ or $B\bar{B}$ thresholds.

Many quarkonium-like states were found in the energy scans of the cross sections of e^+e^- annihilation into conventional quarkonia and light hadrons. Among these are the $Y(4008)$ and $Y(4260)$ in $J/\psi\pi^+\pi^-$ [4], the $Y(4360)$ and $Y(4660)$ in $\psi(2S)\pi^+\pi^-$ [5], the $\psi(4040)$ and $\psi(4160)$ in $J/\psi\eta$ [6], and possibly the $Y(4220)$ in $h_c\pi^+\pi^-$ [7]. The partial widths of the corresponding transitions are much higher than expected for conventional quarkonia [8]. Surprisingly, the peaks observed in the cross sections depend on the final states. In other words, each such charmonium-like state decays to only one channel with charmonium. To explain this “selectivity”, a hadrocharmonium notion is introduced [9]: a bound state of a charmonium and a light hadron. Such a system decays predominantly into its constituents.

Recent energy scans of the $e^+e^- \rightarrow \Upsilon(nS)\pi^+\pi^-$ ($n = 1, 2, 3$) cross sections by Belle [10, 11] show that the situation is different in the sector of bottomonium-like states: all of the cross sections exhibit peaks of the $\Upsilon(10860)$ and $\Upsilon(11020)$ resonances that are also seen in the total hadronic cross section. The observed decay patterns of $\Upsilon(10860)$ and $\Upsilon(11020)$ agree with the expectations for a mixture of the $B_{(s)}^{(*)}\bar{B}_{(s)}^{(*)}$ molecule and conventional bottomonium: open flavor channels dominate, while channels with quarkonium have anomalously high partial widths [12]. The striking difference between charmonium-like and bottomonium-like states is not yet understood. Further scans in the bottomonium region are therefore of high importance. In this Letter, we report the first energy scan of the $e^+e^- \rightarrow h_b(nP)\pi^+\pi^-$ ($n = 1, 2$) cross sections. We find clear $\Upsilon(10860)$ and $\Upsilon(11020)$ peaks without a significant continuum contribution.

To date, the $e^+e^- \rightarrow h_b(nP)\pi^+\pi^-$ processes were seen only at a single energy near the $\Upsilon(10860)$ peak [13]. They were found to proceed entirely via the intermediate isovector states $Z_b(10610)$ and $Z_b(10650)$ that are situated near the $B\bar{B}^*$ and $B^*\bar{B}^*$ thresholds [14] and likely have corresponding molecular structures [15]. Here, we report on the resonant substructure study of the $\Upsilon(11020) \rightarrow h_b(nP)\pi^+\pi^-$ decays, where we find first evidence for intermediate Z_b states. Hereinafter, the $\Upsilon(10860)$ and $\Upsilon(11020)$ are referred to, for brevity, as the $\Upsilon(5S)$ and $\Upsilon(6S)$ according to the potential model assignment.

We use 121.4 fb^{-1} of on-resonance $\Upsilon(5S)$ data taken at three energies close to 10.866 GeV , as well as 1 fb^{-1} of data taken at each of 19 different energies between 10.77 and 11.02 GeV . These data were collected with the Belle detector [16] at the KEKB asymmetric-energy e^+e^- collider [17].

The $e^+e^- \rightarrow h_b(nP)\pi^+\pi^-$ processes are reconstructed inclusively based on the $\pi^+\pi^-$ missing mass, $M_{\text{miss}}(\pi\pi) = \sqrt{(E_{\text{c.m.}} - E_{\pi\pi}^*)^2 - p_{\pi\pi}^{*2}}$, where $E_{\text{c.m.}}$ is the

center-of-mass (c.m.) energy and $E_{\pi\pi}^*$ and $p_{\pi\pi}^*$ are the energy and momentum of the $\pi^+\pi^-$ pair as measured in the c.m. frame. The c.m. energy is calibrated using the $e^+e^- \rightarrow \Upsilon(nS)\pi^+\pi^- \rightarrow \mu^+\mu^-\pi^+\pi^-$ and $e^+e^- \rightarrow \mu^+\mu^-$ processes, as described in Ref. [11]. This analysis closely follows previous Belle publications [13, 14, 18].

We use a general hadronic event selection with requirements on the position of the primary vertex, track multiplicity, and the total energy and momentum of the event [19]. These criteria suppress Bhabha, $\mu^+\mu^-$, $\tau^+\tau^-$, two-photon and beam-gas processes. Continuum $e^+e^- \rightarrow q\bar{q}$ ($q = u, d, s, c$) events have jet-like shapes in contrast to the spherically symmetric signal events and are suppressed by a requirement on the ratio of the second to zeroth Fox-Wolfram moments: $R_2 < 0.3$ [20]. We only consider positively identified $\pi^+\pi^-$ candidates that originate from the interaction point region.

The measurements of the cross sections are performed with an additional requirement on the *single-pion* π^\pm missing mass,

$$10.59\text{ GeV}/c^2 < M_{\text{miss}}(\pi^\pm) < 10.67\text{ GeV}/c^2, \quad (1)$$

which selects signal events proceeding via the intermediate $Z_b(10610)$ or $Z_b(10650)$ states. We combine the $M_{\text{miss}}(\pi\pi)$ distribution for π^+ satisfying (1) and that for π^- satisfying (1). The $\pi^+\pi^-$ pairs with both $M_{\text{miss}}(\pi^+)$ and $M_{\text{miss}}(\pi^-)$ in the Z_b mass window are counted twice. (If they are counted only once, the combinatorial background develops a dip slightly above the $h_b(2P)$ signal, making the background parameterization difficult.) We take the double entries into account by correcting the errors of the $M_{\text{miss}}(\pi\pi)$ histogram and, based on Monte Carlo (MC) simulation, the $h_b(2P)$ signal yields.

We fit the $M_{\text{miss}}(\pi\pi)$ distribution in the $h_b(1P)$ and $h_b(2P)$ intervals, defined as $9.8\text{ GeV}/c^2 - 10.0\text{ GeV}/c^2$ and $10.17\text{ GeV}/c^2 - 10.34\text{ GeV}/c^2$, respectively. The fit function is the sum of the $h_b(nP)$ signal and combinatorial- and peaking-background components. The shapes of the $h_b(nP)$ signals are determined by convolving the probability density of the initial state radiation (ISR) process with the experimental resolution, described by a Gaussian. We use the ISR probability, calculated up to the second order [21], and take into account the energy dependence of the $e^+e^- \rightarrow h_b(nP)\pi^+\pi^-$ cross sections using an iterative procedure. The resolution is determined using the exclusively reconstructed decays $\Upsilon(5S) \rightarrow \Upsilon(nS)\pi^+\pi^-$, $\Upsilon(nS) \rightarrow \mu^+\mu^-$ to be $(6.84 \pm 0.13)\text{ MeV}/c^2$ for the $h_b(1P)$ and $(6.15 \pm 0.22)\text{ MeV}/c^2$ for the $h_b(2P)$. The resolution is dominated by c.m. energy smearing. The $h_b(nP)$ masses are fixed at the previous Belle measurement [18]. We normalize the signal density functions in such a way that the measured $h_b(nP)$ yields include the ISR correction, $1 + \delta_{\text{ISR}}$, and can be used directly to measure the Born cross sections. The combinatorial background is described by a fourth-order

Chebyshev polynomial in both fit intervals. The order is chosen by maximizing the confidence level of the fit.

Using MC simulation, we find that combining a random pion that satisfies the Z_b mass requirement and a signal pion from $Z_b \rightarrow h_b(nP)\pi$ produces a broad bump under the $h_b(nP)$ signal. This background is incorporated within the combinatorial background and results in minor corrections in the $h_b(1P)$ and $h_b(2P)$ yields of 0.99 ± 0.01 and 0.995 ± 0.005 , respectively. The $\pi^+\pi^-$ pairs originating from the $\Upsilon(2S) \rightarrow \Upsilon(1S)\pi^+\pi^-$ transitions with the $\Upsilon(2S)$ produced inclusively or via ISR result in a peak at $E_{\text{c.m.}} - [m_{\Upsilon(2S)} - m_{\Upsilon(1S)}]$ that is inside the $h_b(2P)$ fit interval for the c.m. energies close to the $\Upsilon(5S)$. The shape of this peaking background is found to be a Gaussian with $\sigma = 11 \text{ MeV}/c^2$. Its normalization is floated in the fit.

To determine the reconstruction efficiency, we use phase-space-generated MC, weighted in $M_{\text{miss}}(\pi)$ according to the fit results for the $\Upsilon(5S) \rightarrow h_b(1P)\pi^+\pi^-$ transitions [14] and in angular variables according to the expectations for the Z_b spin-parity $J^P = 1^+$ [22]. The efficiencies for the $h_b(1P)\pi^+\pi^-$ and $h_b(2P)\pi^+\pi^-$ channels are in the range 40–55% and 35–50%, respectively; they rise with c.m. energy. At the lowest energy point, there is a drop of efficiency by a factor of two since this point is close to the kinematic boundary and the pion momenta are low.

At each energy, the Born cross section is determined according to the formula:

$$\sigma^B(e^+e^- \rightarrow h_b(nP)\pi^+\pi^-) = \frac{N}{L \varepsilon |1 - \Pi|^2}, \quad (2)$$

where N is the number of signal events determined from the $M_{\text{miss}}(\pi\pi)$ fit that includes the ISR correction, L is the integrated luminosity, ε is the reconstruction efficiency and $|1 - \Pi|^2$ is the vacuum polarization correction [23], which is in the range 0.927–0.930. The resulting cross sections are shown in Fig. 1. The cross sections, averaged over the three high statistics on-resonance points at $E_{\text{c.m.}} = (10865.6 \pm 2.0) \text{ MeV}$, are

$$\sigma^B(e^+e^- \rightarrow h_b(1P)\pi^+\pi^-) = 1.66 \pm 0.09 \pm 0.10 \text{ pb}, \quad (3)$$

$$\sigma^B(e^+e^- \rightarrow h_b(2P)\pi^+\pi^-) = 2.70 \pm 0.17 \pm 0.19 \text{ pb}. \quad (4)$$

The ratio of the cross sections is $0.616 \pm 0.052 \pm 0.017$. Here and elsewhere in this Letter, the first uncertainties are statistical and the second are systematic.

The systematic uncertainties in the signal yields originate from the signal and background shapes. The relative uncertainty due to the $M_{\text{miss}}(\pi\pi)$ resolution is correlated among different energy points and is equal to 1.4% for the $h_b(1P)$ and 3.3% for the $h_b(2P)$. The uncertainties due to the $h_b(nP)$ masses and ISR tail shapes are found to be negligible. To estimate the background-shape contribution, we vary the fit interval limits by about 50 MeV

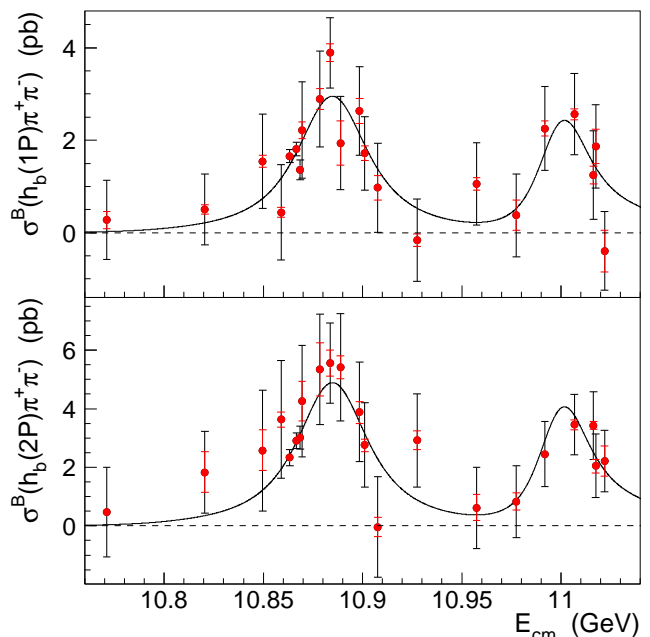


FIG. 1. (colored online) The cross sections for the $e^+e^- \rightarrow h_b(1P)\pi^+\pi^-$ (top) and $e^+e^- \rightarrow h_b(2P)\pi^+\pi^-$ (bottom) as functions of c.m. energy. Points with error bars are the data; outer error bars indicate statistical uncertainties and inner red error bars indicate uncorrelated systematic uncertainties. The solid curves are the fit results.

and the polynomial order for each fit interval. The corresponding uncertainties are considered uncorrelated and are 1.1% and 2.5% for the on-resonance cross sections in Eqs. (3) and (4), respectively.

A relative uncertainty in the efficiency contributes to the correlated systematic uncertainty. An uncertainty due to the Z_b mass requirement of $^{+1.0}_{-1.8}\%$ is estimated by varying the Z_b parameters by $\pm 1\sigma$ and taking into account correlations among different parameters. The efficiency of the R_2 requirement is studied using inclusively reconstructed $\Upsilon(5S) \rightarrow \Upsilon(nS)\pi^+\pi^-$ decays. We find good agreement between data and MC and assign the 5% statistical uncertainty in data as a systematic uncertainty due to the R_2 requirement. Finally, we assign a 1% uncertainty per track due to possible differences in the reconstruction efficiency between data and MC.

An uncertainty in the luminosity of 1.4% is primarily due to the simulation of Bhabha scattering that is used for its determination and is correlated among energy points. We add in quadrature all the contributions to find the total systematic uncertainties shown in Eqs. (3) and (4). The values of the cross sections for all energy points are provided in Ref. [24].

The shapes of the $h_b(1P)\pi^+\pi^-$ and $h_b(2P)\pi^+\pi^-$ cross sections look very similar. They show clear $\Upsilon(5S)$ and $\Upsilon(6S)$ peaks without significant continuum contributions. We perform a simultaneous fit of the shapes,

adding in quadrature the statistical and uncorrelated systematic uncertainties at each energy point. We use the coherent sum of two Breit-Wigner amplitudes:

$$A_n \Phi_n(s) |F_{\text{BW}}(s, M_5, \Gamma_5) + a e^{i\phi} F_{\text{BW}}(s, M_6, \Gamma_6)|^2, \quad (5)$$

where $s \equiv E_{\text{c.m.}}^2$, $\Phi_n(s)$ is the phase space calculated numerically, taking into account the measured Z_b line shape [14], and $F_{\text{BW}}(s, M, \Gamma) = M\Gamma/(s - M^2 + iM\Gamma)$ is a Breit-Wigner amplitude. The fit parameters M_5 , Γ_5 , M_6 , Γ_6 , a and ϕ are common for the two channels, while only the normalization coefficients A_n are different. Equation (5) is convolved with the $E_{\text{c.m.}}$ resolution of (5.0 ± 0.4) MeV, which is found using exclusively reconstructed $\Upsilon(5S) \rightarrow \Upsilon(nS)\pi^+\pi^-$ events. The fitted functions are shown in Fig. 1. The confidence level of the fit is 93%. The fit results are:

$$M_5 = (10884.7_{-3.4}^{+3.6+8.9}) \text{ MeV}/c^2, \quad (6)$$

$$\Gamma_5 = (40.6_{-8.0}^{+12.7+1.1}) \text{ MeV}, \quad (7)$$

$$M_6 = (10999.0_{-7.8}^{+7.3+16.9}) \text{ MeV}/c^2, \quad (8)$$

$$\Gamma_6 = (27_{-11}^{+27+5}) \text{ MeV}, \quad (9)$$

$$a = 0.65_{-0.12}^{+0.36+0.17} \text{ and } \phi = (0.1_{-0.8}^{+0.4} \pm 0.3) \pi. \quad (10)$$

The measured masses and widths agree with the results of the $\Upsilon(nS)\pi^+\pi^-$ scan [11].

The first error in the fit results is not purely statistical but includes uncorrelated systematic uncertainties in the cross sections. The contributions of other considered sources are listed in Table I.

TABLE I. The systematic uncertainties in the $\Upsilon(5S)$ and $\Upsilon(6S)$ masses (in MeV/c^2), widths (in MeV), amplitude a , and phase ϕ (in units of π).

	M_5	Γ_5	M_6	Γ_6	a	ϕ
Fit model	+8.9 -0.1	+0.4 -19.1	+16.7 -0.0	+0.0 -11.5	+0.12 -0.00	+0.09 -0.00
Z_b substructure	+0.2 -0.0	+0.0 -0.2	+0.1 -0.0	+0.7 -0.0	+0.11 -0.00	+0.00 -0.29
\sqrt{s} scale	1.0	1.0	+3.0 -1.0	+4.7 -1.0	+0.00 -0.10	+0.25 -0.00
Resolution	0.0	+0.3 -0.2	0.1	0.6	0.0	+0.01 -0.00
Total	+8.9 -1.0	+1.1 -19.1	+16.9 -1.0	+4.8 -11.5	+0.17 -0.10	+0.27 -0.29

To study systematic uncertainties due to the fit model, we introduce a non-resonant continuum amplitude, $b e^{i\delta}$. The significance of this contribution is only 1.6σ . However, the shifts in the fit results are large, and this is the dominant source of systematic uncertainty. We also consider the possibility that the parameters a and ϕ are different in the $h_b(1P)\pi^+\pi^-$ and $h_b(2P)\pi^+\pi^-$ channels. We find that the values in the two channels agree and the shifts in masses and widths are small. Using MC pseudo-experiments, we find that there is no significant fit bias.

If the resonant substructures of the $\Upsilon(5S)$ and $\Upsilon(6S)$ decays are different, the $\Upsilon(5S)$ and $\Upsilon(6S)$ amplitudes

in (5) are not fully coherent, and the interference term is suppressed by a decoherence factor k [11]. If only $Z_b(10610)$ is produced at the $\Upsilon(6S)$, k is calculated numerically to be 0.62; if only $Z_b(10650)$ is produced, k is 0.80. We introduce these factors in the fit and take into account that the efficiency of the Z_b mass requirement is smaller for a single Z_b state compared to two Z_b states by 12% since the two Z_b states interfere destructively outside their signal region.

We account for an uncertainty in the $E_{\text{c.m.}}$ scale and the uncertainty in the $E_{\text{c.m.}}$ resolution. We add in quadrature the contributions of the various sources to determine the total systematic uncertainties.

To study the resonant substructure of the $\Upsilon(6S) \rightarrow h_b(nP)\pi^+\pi^-$ transitions, we combine the data samples of the five highest-energy points. The fits to the corresponding $M_{\text{miss}}(\pi\pi)$ spectra in the $h_b(1P)$ and $h_b(2P)$ intervals are shown in Figs. 2 and 3. The $h_b(nP)$ sig-

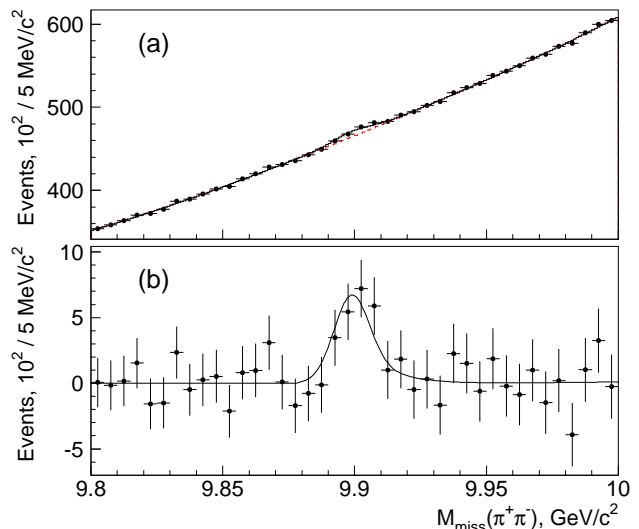


FIG. 2. (colored online) The $M_{\text{miss}}(\pi\pi)$ spectrum in the $h_b(1P)$ region for the combined data samples of five energy points near the $\Upsilon(6S)$. In (a) the data are the points with error bars with the fit function (solid curve) and background (red dashed curve) overlaid. (b) shows the background-subtracted data (points with error bars) with the signal component of the fit overlaid (solid curve).

nal density functions are determined by averaging over the data samples that are combined; we use weights proportional to the integrated luminosity and the cross section at each energy. The confidence levels of the fits are 50% and 52%, respectively. From Wilks' theorem [25], we find that the significances of the $h_b(1P)$ and $h_b(2P)$ signals are 3.5σ and 5.3σ , respectively, including systematic uncertainty, determined by varying the polynomial order. Thus, we find the first evidence for the $\Upsilon(6S) \rightarrow h_b(1P)\pi^+\pi^-$ transition and observe for the first time the $\Upsilon(6S) \rightarrow h_b(2P)\pi^+\pi^-$ transition.

We release the requirement of an intermediate Z_b and

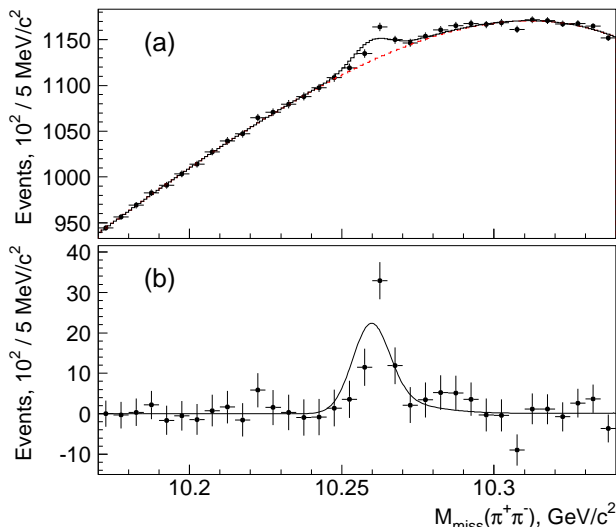


FIG. 3. (colored online) The $M_{\text{miss}}(\pi\pi)$ spectrum in the $h_b(2P)$ interval for the combined data samples of five energy points near the $\Upsilon(6S)$. The legend is the same as in Fig. 2.

fit the $M_{\text{miss}}(\pi\pi)$ spectra in bins of $M_{\text{miss}}(\pi)$ to measure the $h_b(nP)\pi^+\pi^-$ yields as functions of $M_{\text{miss}}(\pi)$. The distribution of the phase-space-generated signal events in the $M_{\text{miss}}(\pi^+)$ vs. $M_{\text{miss}}(\pi^-)$ plane has the shape of a narrow slanted band; each structure at high values of $M_{\text{miss}}(\pi^\pm)$ produces a “reflection” at small values of $M_{\text{miss}}(\pi^\mp)$. We combine the $M_{\text{miss}}(\pi\pi)$ spectra for the corresponding $M_{\text{miss}}(\pi^+)$ and $M_{\text{miss}}(\pi^-)$ bins and consider the upper half of the available $M_{\text{miss}}(\pi)$ range. Thereby, we consider all signal events and avoid double counting. The yields, corrected for the reconstruction efficiencies, are shown in Fig. 4. The data are not

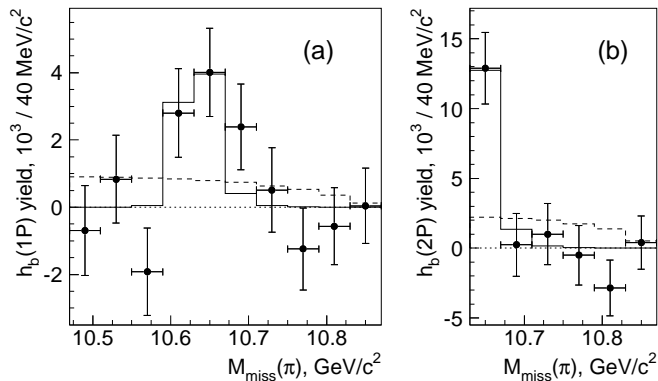


FIG. 4. The efficiency-corrected yields of $h_b(1P)\pi^+\pi^-$ (a) and $h_b(2P)\pi^+\pi^-$ (b) as functions of $M_{\text{miss}}(\pi)$ for the combined data samples of five energy points in the $\Upsilon(6S)$ region. Points represent data; the solid histogram represents the fit result with the Z_b signal shape fixed from the $\Upsilon(5S)$ analysis; the dashed histogram represents the result of the fit with a phase space distribution.

distributed uniformly in phase space; they populate the

$Z_b(10610)$ and $Z_b(10650)$ mass region. We fit the data to a shape where the $Z_b(10610)$ and $Z_b(10650)$ parameters are fixed to the $\Upsilon(5S) \rightarrow Z_b\pi \rightarrow h_b(1P)\pi^+\pi^-$ result and the non-resonant contribution is set to zero [14]. Such a model describes the data well: the confidence levels of the fits are 65% and 77% for the $h_b(1P)$ and $h_b(2P)$, respectively. The phase space hypothesis is excluded relative to this model at the 3.6σ and 4.5σ levels in the $h_b(1P)\pi^+\pi^-$ and $h_b(2P)\pi^+\pi^-$ channels, respectively. The single $Z_b(10610)$ hypothesis is excluded at the 3.3σ level in the $h_b(1P)\pi^+\pi^-$ channel, while the single $Z_b(10650)$ hypothesis cannot be excluded at a significant level. In the $h_b(2P)\pi^+\pi^-$ channel, the $Z_b(10610)^\pm$ and $Z_b(10650)^\pm$ signals overlap with the $Z_b(10650)^\mp$ and $Z_b(10610)^\mp$ reflections, respectively, which obscures the determination of the relative yields. The exclusion levels are determined using pseudo-experiments from the χ^2 differences of the two hypotheses being compared, and include systematic uncertainty.

In conclusion, we have measured the energy dependence of the $e^+e^- \rightarrow h_b(nP)\pi^+\pi^-$ ($n = 1, 2$) cross sections. We find two peaks corresponding to the $\Upsilon(5S)$ and $\Upsilon(6S)$ states and measure their parameters, which agree with the results from Ref. [11]. The data are consistent with no continuum contribution.

We report first evidence for $\Upsilon(6S) \rightarrow h_b(1P)\pi^+\pi^-$ and first observation of the $\Upsilon(6S) \rightarrow h_b(2P)\pi^+\pi^-$ transitions. We study their resonant substructures and find evidence that they proceed entirely via the intermediate isovector states $Z_b(10610)$ and $Z_b(10650)$. Their relative fraction is loosely constrained by the current data: the hypothesis that only $Z_b(10610)$ is produced is excluded at the 3.3σ level, while the hypothesis that only $Z_b(10650)$ is produced is not excluded at a significant level.

The shapes of the $e^+e^- \rightarrow h_b(nP)\pi^+\pi^-$ and $e^+e^- \rightarrow \Upsilon(nS)\pi^+\pi^-$ cross sections look similar. The only significant difference is a smaller relative yield of $\Upsilon(nS)\pi^+\pi^-$ at the $\Upsilon(6S)$. Since the $h_b(nP)\pi^+\pi^-$ final states are produced only via intermediate Z_b while $\Upsilon(nS)\pi^+\pi^-$ at the $\Upsilon(5S)$ are produced both via Z_b and non-resonantly, this difference indicates that the non-resonant contributions in $\Upsilon(nS)\pi^+\pi^-$ are suppressed at the $\Upsilon(6S)$.

We thank the KEKB group for excellent operation of the accelerator; the KEK cryogenics group for efficient solenoid operations; and the KEK computer group, the NII, and PNNL/EMSL for valuable computing and SINET4 network support. We acknowledge support from MEXT, JSPS and Nagoya’s TLPRC (Japan); ARC (Australia); FWF (Austria); NSFC and CCEPP (China); MSMT (Czechia); CZF, DFG, EXC153, and VS (Germany); DST (India); INFN (Italy); MOE, MSIP, NRF, BK21Plus, WCU and RSRI (Korea); MNIW and NCN (Poland); MES, RFAAE and RSF under Grant No. 15-12-30014 (Russia); ARRS (Slovenia); IKERBASQUE and UPV/EHU (Spain); SNSF (Switzerland); MOE and MOST (Taiwan); and DOE and NSF (USA).

-
- [1] N. Brambilla *et al.*, Eur. Phys. J. C **71**, 1534 (2011).
- [2] S.K. Choi *et al.* [Belle Collaboration], Phys. Rev. Lett. **91**, 262001 (2003).
- [3] K.A. Olive *et al.* [Particle Data Group], Chin. Phys. C **38**, 090001 (2014).
- [4] J.P. Lees *et al.* [BaBar Collaboration], Phys. Rev. D **86**, 051102 (2012); Z.Q. Liu *et al.* [Belle Collaboration], Phys. Rev. Lett. **110**, 252002 (2013).
- [5] J.P. Lees *et al.* [BaBar Collaboration], Phys. Rev. D **89**, 111103 (2014); X. L. Wang *et al.* [Belle Collaboration], Phys. Rev. D **91**, 112007 (2015).
- [6] X. L. Wang *et al.* [Belle Collaboration], Phys. Rev. D **87**, 051101 (2013); M. Ablikim *et al.* [BESIII Collaboration], Phys. Rev. D **91**, 112005 (2015).
- [7] M. Ablikim *et al.* [BESIII Collaboration], Phys. Rev. Lett. **111**, 242001 (2013); C.Z. Yuan, Chin. Phys. C **38**, 043001 (2014).
- [8] N. Brambilla *et al.*, Eur. Phys. J. C **74**, 2981 (2014).
- [9] S. Dubynskiy and M. B. Voloshin, Phys. Lett. B **666**, 344 (2008).
- [10] K.-F. Chen *et al.* [Belle Collaboration], Phys. Rev. D **82**, 091106 (2010).
- [11] D. Santel *et al.* [Belle Collaboration], Phys. Rev. D **93**, 011101 (2016).
- [12] M. B. Voloshin, Phys. Rev. D **85**, 034024 (2012).
- [13] I. Adachi *et al.* [Belle Collaboration], Phys. Rev. Lett. **108**, 032001 (2012).
- [14] A. Bondar *et al.* [Belle Collaboration], Phys. Rev. Lett. **108**, 122001 (2012).
- [15] A. Bondar *et al.*, Phys. Rev. D **84**, 054010 (2011).
- [16] A. Abashian *et al.* [Belle Collaboration], Nucl. Instrum. Meth. A **479**, 117 (2002); also see detector section in J. Brodzicka *et al.*, Prog. Theor. Exp. Phys. **2012**, 04D001 (2012).
- [17] S. Kurokawa and E. Kikutani, Nucl. Instrum. Meth. A **499**, 1 (2003), and other papers included in this Volume; T. Abe *et al.*, Prog. Theor. Exp. Phys. **2013**, 03A001 (2013) and references therein.
- [18] R. Mizuk *et al.* [Belle Collaboration], Phys. Rev. Lett. **109**, 232002 (2012).
- [19] K. Abe *et al.* [Belle Collaboration], Phys. Rev. D **64**, 072001 (2001).
- [20] G.C. Fox and S. Wolfram, Phys. Rev. Lett. **41**, 1581 (1978).
- [21] E.A. Kuraev and V.S. Fadin, Sov. J. Nucl. Phys. **41**, 466 (1985); M. Benayoun, S.I. Eidelman, V.N. Ivanchenko and Z.K. Silagadze, Mod. Phys. Lett. A **14**, 2605 (1999).
- [22] A. Garmash *et al.* [Belle Collaboration], Phys. Rev. D **91**, 072003 (2015).
- [23] S. Actis *et al.*, Eur. Phys. J. C **66**, 585 (2010).
- [24] See Supplemental Material at [URL will be inserted by publisher] for tables of $\sigma^B[e^+e^- \rightarrow h_b(nP)\pi^+\pi^-]$ ($n = 1, 2$) measurements.
- [25] S.S. Wilks, Ann. Math. Statist. **9**, 60 (1938). DOI:10.1214/aoms/1177732360.

Supplemental Material

1 The $e^+e^- \rightarrow h_b(nP)\pi^+\pi^-$ ($n = 1, 2$) Born cross sections for all energy points are presented in Table I.

2 TABLE I. Center-of-mass energies, integrated luminosities and Born cross sections for all energy points. The first uncertainty
3 in the energy is uncorrelated, the second is correlated. The three uncertainties in the cross sections are statistical, uncorrelated
4 systematic and correlated systematic.

#	\sqrt{s} , MeV	Luminosity, fb $^{-1}$	$\sigma(e^+e^- \rightarrow h_b(1P)\pi^+\pi^-)$, pb	$\sigma(e^+e^- \rightarrow h_b(2P)\pi^+\pi^-)$, pb
1	$11022.0_{-5.3}^{+0.4} \pm 1.0$	0.98	$-0.39 \pm 0.85 \pm 0.45 \pm 0.02$	$2.21 \pm 1.05 \pm 0.51 \pm 0.15$
2	$11017.5 \pm 4.0 \pm 1.0$	0.86	$1.87 \pm 0.90 \pm 0.37 \pm 0.11$	$2.05 \pm 1.09_{-0.24}^{+0.21} \pm 0.14$
3	$11016.4_{-4.6}^{+0.4} \pm 1.0$	0.77	$1.25 \pm 0.96 \pm 0.19 \pm 0.08$	$3.42 \pm 1.15_{-0.13}^{+0.15} \pm 0.23$
4	$11006.8_{-3.9}^{+0.4} \pm 1.0$	0.98	$2.57 \pm 0.88 \pm 0.13 \pm 0.15$	$3.45 \pm 1.03 \pm 0.17 \pm 0.23$
5	$10991.9 \pm 0.4 \pm 1.0$	0.99	$2.25 \pm 0.91 \pm 0.16 \pm 0.14$	$2.45 \pm 1.11 \pm 0.13 \pm 0.17$
6	$10977.5 \pm 0.4 \pm 1.0$	1.00	$0.38 \pm 0.90 \pm 0.33 \pm 0.02$	$0.83 \pm 1.23 \pm 0.29 \pm 0.06$
7	$10957.5 \pm 4.0 \pm 1.0$	0.97	$1.05 \pm 0.89 \pm 0.14 \pm 0.06$	$0.60 \pm 1.39_{-0.42}^{+0.47} \pm 0.04$
8	$10927.5 \pm 4.0 \pm 1.0$	1.15	$-0.16 \pm 0.89 \pm 0.13 \pm 0.01$	$2.92 \pm 1.59 \pm 0.33 \pm 0.20$
9	$10907.7_{-4.9}^{+0.4} \pm 1.0$	0.98	$0.97 \pm 0.96 \pm 0.27 \pm 0.06$	$-0.04 \pm 1.72 \pm 0.33 \pm 0.00$
10	$10901.1_{-4.9}^{+1.1} \pm 1.0$	1.42	$1.72 \pm 0.79 \pm 0.16 \pm 0.10$	$2.76 \pm 1.44_{-0.24}^{+0.20} \pm 0.19$
11	$10898.5_{-4.0}^{+0.4} \pm 1.0$	0.98	$2.63 \pm 0.96 \pm 0.27 \pm 0.16$	$3.89 \pm 1.70_{-0.40}^{+0.35} \pm 0.26$
12	$10888.9_{-2.0}^{+0.4} \pm 1.0$	0.99	$1.94 \pm 1.00 \pm 0.48 \pm 0.12$	$5.41 \pm 1.83 \pm 0.40 \pm 0.37$
13	$10883.6_{-2.1}^{+0.9} \pm 1.0$	1.85	$3.89 \pm 0.76 \pm 0.19 \pm 0.23$	$5.55 \pm 1.37 \pm 0.45 \pm 0.38$
14	$10878.5_{-1.4}^{+0.4} \pm 1.0$	0.98	$2.89 \pm 1.04 \pm 0.23 \pm 0.17$	$5.34 \pm 1.89 \pm 0.91 \pm 0.36$
15	$10869.5_{-2.0}^{+0.4} \pm 1.0$	0.98	$2.22 \pm 1.04 \pm 0.18 \pm 0.13$	$4.26 \pm 1.90 \pm 0.68 \pm 0.29$
16	$10868.6 \pm 0.2 \pm 0.5$	22.94	$1.36 \pm 0.21 \pm 0.04 \pm 0.08$	$3.01 \pm 0.39 \pm 0.08 \pm 0.20$
17	$10866.7 \pm 0.2 \pm 0.5$	50.47	$1.81 \pm 0.15 \pm 0.04 \pm 0.11$	$2.91 \pm 0.26 \pm 0.08 \pm 0.20$
18	$10863.3 \pm 0.2 \pm 0.5$	47.65	$1.66 \pm 0.15 \pm 0.03 \pm 0.10$	$2.33 \pm 0.27 \pm 0.11 \pm 0.16$
19	$10858.9_{-2.0}^{+0.4} \pm 1.0$	0.99	$0.44 \pm 1.03 \pm 0.11 \pm 0.03$	$3.63 \pm 2.01_{-0.27}^{+0.25} \pm 0.25$
20	$10849.7_{-1.2}^{+0.4} \pm 1.0$	0.99	$1.54 \pm 1.02 \pm 0.13 \pm 0.09$	$2.57 \pm 2.07_{-0.68}^{+0.71} \pm 0.17$
21	$10820.5_{-0.4}^{+6.5} \pm 1.0$	1.70	$0.50 \pm 0.77 \pm 0.10 \pm 0.03$	$1.83 \pm 1.40 \pm 0.70 \pm 0.12$
22	$10771.1 \pm 1.8 \pm 1.0$	0.95	$0.28 \pm 0.86 \pm 0.19 \pm 0.02$	$0.47 \pm 1.52 \pm 0.12 \pm 0.03$